S. H. Advani
Professor and Chairman.

J. K. Lee
Department of Engineering Mechanics,
The Ohio State University,
Columbus, Ohio 43210

H. F. Wang
Fluor Corporation,
Irvine, Calif. 92730

Thermo-Elastic Responses Associated With Cavities and Cracks in Infinite Media

The increased adaption of classical thermo-elasticity solutions for rock mechanics applications has been evident in recent years. In this paper, specialized thermo-elastic solutions for a triaxial ellipsoidal cavity with uniform surface temperature are presented and results for several limiting cases are deduced. For completeness and comparison, solutions and results for the related thermally stressed problem of a prolate spheroidal cavity are detailed. In addition, the applicability of the finite element technique and an appropriate failure criteria for in-situ thermo-mechanical problems is indicated.

Introduction

The quest for innovative techniques for energy resource extraction has focused considerable attention on various thermally related recovery procedures. Optimum in-situ energy recovery from coal [1], oil shale [2, 3], tar sands and geothermal reservoirs [4, 5] necessitates evaluations of temperature profiles and induced stress/fracture responses associated with cavities and cracks in sedimentary rock. A selected bibliography on rock thermo-physical and thermo-mechanical properties along with a state-of-the-art review of numerical response models has been recently published by the National Academy of Sciences [6]. For rock mechanics applications, it is indicated that closed form solutions provide not only a versatile and economical tool for analysis, but also a sound base for validation of more general numerical models. An increased usage of classical thermo-elasticity solutions for response calibration and model scaling prior to sophisticated numerical or experimental simulations of complex problems has been recently evident.

Pertinent investigations related to the determination of thermal stresses in infinite bodies include studies on hot, prolate spheroid-shaped inclusions [7, 8] and insulated ovaloid and spheroidal cavities [9, 10]. Several two-dimensional crack problems with thermal loading have also been investigated [11–14]. Closed form thermo-elastic solutions for three-dimensional crack problems subjected to uniform temperature or heat flux loading have been reported by Olesiak and Sneddon [15], Kassir and Sih [16] and Kassir [17, 18]. Recently, Advani and Wang [19] have obtained explicit expressions for the state of stress associated with an ellipsoidal cavity having uniform surface temperature. These solutions have been specialized to determine the crack opening mode stress intensity factor for elliptic cracks by limiting derivations.

In this paper, the thermo-elastic solutions for a triaxial ellipsoidal cavity with uniform temperature are briefly presented and specialized results for an oblate spheroidal cavity and simplified crack configurations are indicated. Solutions and results for the corresponding three-dimensional problem of a prolate spheroidal cavity are also detailed. The relevance of these problems, for example, is evidenced by the spheroidal or tear drop cavity configurations encountered in underground coal conversion. These cavities generally evolve from a "needlelike" reverse combustion linking channel. The stress intensity factor determinations provide basic information on thermal crack propagation in the thermally disturbed zones. Results demonstrating the use of finite element techniques for sample problems are also presented. In addition, the potential application of a previously derived thermo-mechanical failure criterion is indicated.

Ellipsoidal Cavity Formulations and Special Cases

The ellipsoidal cavity problem represents the general case for various correspondingly stressed cavity/crack configurations. Special cases include the oblate spheroidal and spherical cavities as well as the elliptical, parabolic, circular, and through line crack geometries. Selected formulations and solutions for the ellipsoidal cavity boundary value problem are hence presented here [19].

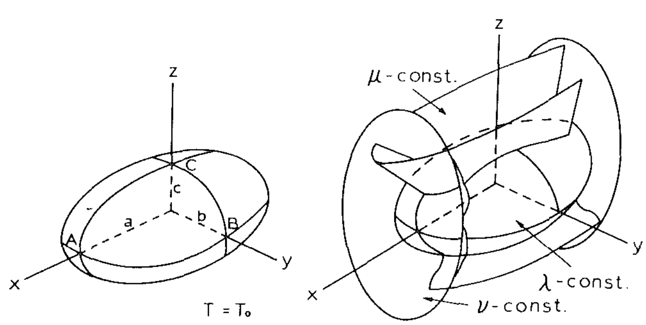

Fig. 1 Ellipsoidal cavity with constant temperature and associated coordinate system

Contributed by the Petroleum Division for publication in the JOURNAL OF ENERGY RESOURCES TECHNOLOGY. Manuscript received by the Petroleum Division, March 27, 1981; revised manuscript received March 16, 1982.

We consider an ellipsoidal cavity in a homogeneous, isotropic, linear elastic medium of infinite extent (Fig. 1). The traction-free cavity surface is maintained at a constant temperature T_o. Vanishing temperature and stress fields are assumed at infinity. The uncoupled thermo-elastic problem, with time-dependent terms ignored, requires the solution of the three-dimensional Laplacian equation

$$\nabla^2 T = 0 \tag{1}$$

and determination of the resulting displacements and stresses from the Navier equations and Duhamel-Neumann constitutive relations

$$\nabla(\nabla \cdot \mathbf{u}) + (1-2\nu^*)\nabla^2\mathbf{u} = 2(1+\nu^*)\alpha\nabla T \tag{2}$$

$$\boldsymbol{\phi} = \mu^*\left\{\nabla\mathbf{u} + \mathbf{u}\nabla + \frac{2}{(1-2\nu^*)}[\nu^*\nabla\cdot\mathbf{u} - (1+\nu^*)\alpha T]\Pi\right\} \tag{3}$$

where $\mathbf{u}$ is the displacement vector, $\boldsymbol{\phi}$ is the stress dyadic, μ^*, ν^* and α denote the shear modulus, Poisson's ratio, and coefficient of linear thermal expansion, respectively, and Π is the unit dyadic.

The solution to equation (1) with the temperature $T = T_o$ at the cavity surface $\lambda = \lambda_o$ and vanishing at infinity ($\lambda = 0$) is

$$T = \frac{T_o \lambda}{\lambda_o} \tag{4}$$

With the temperature field determined, the stress solutions are obtained from the thermo-elastic potential equation associated with the particular solution for the displacement vector and the Papkovitch-Neuber form of the homogeneous stress field. Detailed expressions for the resultant thermo-elastic stress fields are presented by Advani and Wang [19].

For the oblate spheroidal cavity, the expression analogous to equation (4) is

$$T = T_o \frac{\cot^{-1}(\sinh\lambda)}{\cot^{-1}(\sinh\lambda_o)} \tag{5}$$

and the pertinent stress fields can be accordingly deduced from the ellipsoidal cavity expressions with $a = b$.

Specialization of the general ellipsoidal results to the case of a flat ellipsoidal cavity ($c \to 0$) yields the maximum principal stress at A (Fig. 1) [19]

$$(\sigma_1)_{\max} = \frac{-2b(1+\nu^*)}{c(1-\nu^*)} \frac{\alpha\mu^* T_o}{E(k)} \tag{6}$$

This principal stress can also be used to derive the stress intensity factor for the elliptical crack ($c = 0$) by utilizing the definition

$$K_1 = \lim_{\rho \to 0} \frac{(\sigma_1)_{\max}\rho^{1/2}\pi^{1/2}}{2} \tag{7}$$

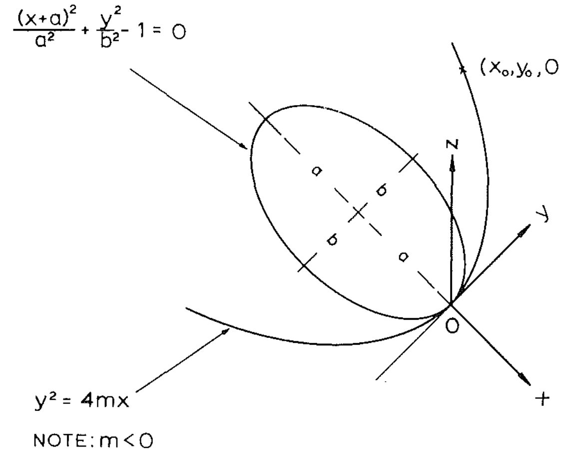

Fig. 2 Transition of elliptical crack to parabolic crack

where $\rho = c^2/(a^2\cos^2\phi + b^2\sin^2\phi)^{1/2}$ is the maximum principal radius of curvature of the ellipsoidal surface at a point $z = 0$ and the coordinate angle ϕ is measured in the elliptical crack plane from the major axis.

Equations (6) and (7) yield the classical result

$$K_I = -\frac{(1+\nu^*)b\alpha\mu^* T_o(\pi)^{1/2}}{(1-\nu^*)E(k)(a^2\cos^2\phi + b^2\sin^2\phi)^{1/4}} \tag{8}$$

The reduction of the elliptic crack to a plane crack bounded by a curve in the shape of a parabola ($y^2 = 4mx$, $z = 0$) is achieved by letting a and $b \to \infty$ (Fig. 2), such that

$$a - (a^2 - b^2)^{1/2} = -m$$

The transition to the parabola simultaneously entails an increase in the eccentricity of the ellipse to unity [20]. The resultant expression is

$$K_I = \frac{-(1+\nu^*)}{(1-\nu^*)}\alpha\mu^* T_o(4m^2 + y_o^2)^{1/4}(\pi)^{1/2} \tag{9}$$

where (x_o, y_o) is a point on the parabolic crack.

Cases represented by the circular crack ($a = b$) and through crack (plane strain case $a \to \infty$) can also be deduced from equation (8). For example, the Mode I stress intensity factor, from equation (8) with $\phi = \pi/2$, is given by

$$K_I = -\frac{(1+\nu^*)}{(1-\nu^*)}\alpha\mu^* T_o\sqrt{\pi b} = -\frac{(1+\nu^*)}{2(1-\nu^*)}\alpha\mu^*\frac{Q_o}{\kappa}\left(\frac{b}{\pi}\right)^{1/2} \tag{10}$$

where Q_o is the equivalent heat flux intensity and κ is the thermal conductivity of the medium.

The results for the plane strain model of an insulated crack

Nomenclature

- a,b,c = semi-axes of the ellipsoid, spheroid ($b = c$), elliptical crack ($c = 0$).
- b = line crack half-length
- A_R, A_I = real and imaginary parts of complex thermal constant
- A_n, B_n = constants
- $E(k)$ = complete elliptical integral of second kind
- K_I, K_{II} = Mode I and Mode II stress intensity factors, respectively
- K_{Ic} = critical Mode I stress intensity factor
- $k = (1 - b^2/a^2)^{1/2}$ = modulus of elliptical integral
- m = focal length of parabolic crack
- M = bulk modulus
- p,q = auxiliary parameters for spheroidal cavity
- p_o = crack internal pressure
- P_n, Q_n = Legendre polynomials of first and second kind, respectively
- S_t = tensile strength
- T = temperature
- $\mathbf{u}$ = displacement vector
- x,y,z = cartesian coordinates
- α = linear thermal expansion coefficient
- λ, μ, ν = orthogonal curvilinear coordinates
- μ^* = shear modulus
- μ_f = internal friction coefficient
- ν^* = Poisson's ratio
- ϕ, ψ = Papkovitch-Neuber functions
- σ_{ij} = stress components
- $\boldsymbol{\phi}$ = stress tensor
- σ_c = critical stress for crack closure
- χ_p = thermo-elastic displacement potential

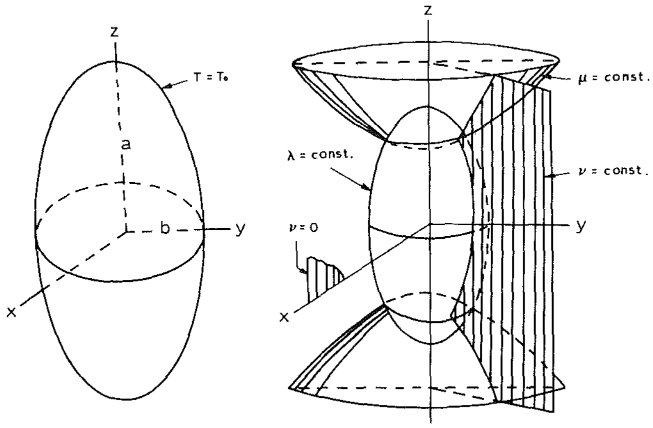

Fig. 3 Prolate spheroidal cavity with constant surface temperature and associated coordinate system

disturbed by a steady-state temperature gradient (∇T) can be similarly deduced from the skew symmetric elliptic crack results of Kassir and Sih [16]. The Mode II stress intensity factor is given by

$$K_{II} = -\frac{(1+\nu^*)}{2(1-\nu^*)}\,\alpha\mu^*(\nabla T)\,b^{3/2}\sin\beta_1 \tag{11}$$

where β_1 is the inclination of the undisturbed heat flow axis with respect to the crack axis.

In lieu of the preceding limiting case derivations, expressions (10) and (11) have been directly obtained [21] from the Kolosoff function complex variable approach reported by Mushkhelishvili [22].

Prolate Spheroidal Cavity Thermo-Elastic Solutions

The prolate spheroidal cavity ($x^2/b^2 + y^2/b^2 + z^2/a^2 = 1$) with uniform temperature T_o prescribed on its surface (Fig. 3) represents extreme configurations ranging from a spherical cavity to a needle crack of finite length. For the problem discussed here, vanishing temperature and stress fields are assumed at infinity. The related problem of thermal stresses induced by the disturbance of uniform heat flow by an insulated spheroidal cavity has been investigated by Florence and Goodier [9]. The solution to the problem, governed by equations (1), (2), and (3), is presented as a function of auxiliary variables corresponding to the prolate spheroidal coordinate system defined by

$$\begin{aligned}
x &= \delta\sinh\lambda\sin\mu\cos\nu = \delta\bar{q}\bar{p}\cos\nu \\
y &= \delta\sinh\lambda\sin\mu\sin\nu = \delta\bar{q}\bar{p}\sin\nu \\
z &= \delta\cosh\lambda\cos\mu = \delta qp \\
q &= \cosh\lambda, \bar{q} = \sinh\lambda = (q^2-1)^{1/2} \\
p &= \cos\mu, \bar{p} = \sin\mu = (1-p^2)^{1/2}
\end{aligned} \tag{12}$$

where $\delta^2 = a^2 - b^2$.

The solution to equation (1) with the temperature $T = T_o$ at the cavity surface $q = q_o$ and vanishing at infinity is

$$T = \frac{T_o}{Q_o(q_o)}Q_o(q) = \frac{T_o}{2Q_o(q_o)}\ln\frac{(q+1)}{(q-1)} \tag{13}$$

Where $Q_o(q)$ is the Legendre function of the second kind of zero degree.

The solution to equation (2) is obtained by expressing the displacement field in the form

$$\mathbf{u} = \mathbf{u}_H + \mathbf{u}_p \tag{14}$$

where $\mathbf{u}_H$ represents the solution to the isothermal, homogeneous form of equation (2) and $\mathbf{u}_p$ is a particular solution to the nonhomogeneous equation (2).

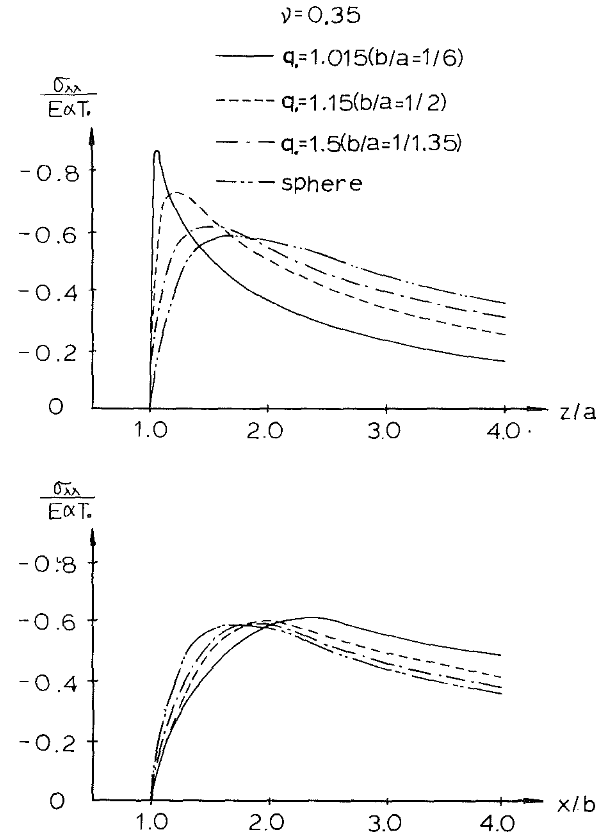

Fig. 4 Nondimensional stress $\sigma_{\lambda\lambda}/E\alpha T_o$ along the z and x axes of the prolate spheroidal cavity

To facilitate determination of $\mathbf{u}_p$, we introduce the thermoelastic displacement potential χ_p defined by

$$\mathbf{u}_p = \delta^2\,\nabla\chi_p \tag{15}$$

Insertion of equation (15) into equation (2) yields

$$\delta^2\,\nabla^2\chi_p = \frac{1+\nu^*}{1-\nu^*}\alpha T \tag{16}$$

The particular solution to equation (16), after inserting equation (13) is found to be

$$\chi_p = \frac{(1+\nu^*)}{6(1-\nu^*)}\frac{\alpha T_o}{Q_o(q_o)}[(p^2+q^2)Q_o(q) + 2q] \tag{17}$$

The $\sigma_{\lambda\lambda}$, $\sigma_{\lambda\nu}$ stress components associated with this thermoelastic potential, determined in terms of Legendre polynomials, are

$$\begin{aligned}
\frac{\sigma_{\lambda\lambda}}{2\mu^*\delta^4h^4\beta} &= R_o(q)P_o(p) + R_2(q)P_2(p) + R_4(q)P_4(p) \\
\frac{\sigma_{\lambda\nu}}{2\mu^*\delta^4h^4\beta} &= \bar{R}_2(q)P_2^1(p) + \bar{R}_4(q)P_4^1(p)
\end{aligned} \tag{18}$$

where

$$R_o(q) = \frac{1}{15}[Q_o(q)(-60q^4 + 40q^2 - 12) + 20q + qQ_o'(q)(30q^4 - 70q^2 + 28)]$$

$$R_2(q) = \frac{1}{12}[Q_o(q)(112q^2 - 28) + qQ_o'(q)(-70q^2 + 82) - 28q]$$

$$R_4(q) = \frac{8}{35}[qQ_o'(q) - 4Q_o(q)]$$

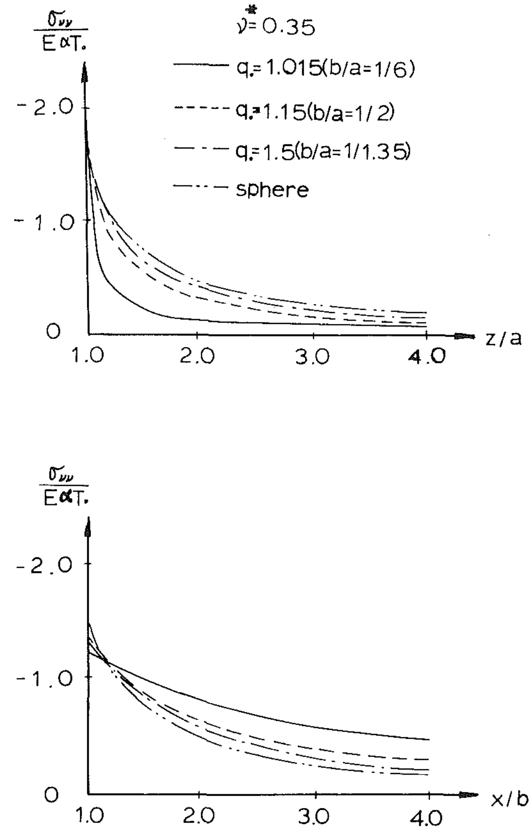

Fig. 5 Nondimensionalized stress $\sigma_{\nu\nu}/E\alpha T_o$ along the z and x axes of the prolate spheroidal cavity

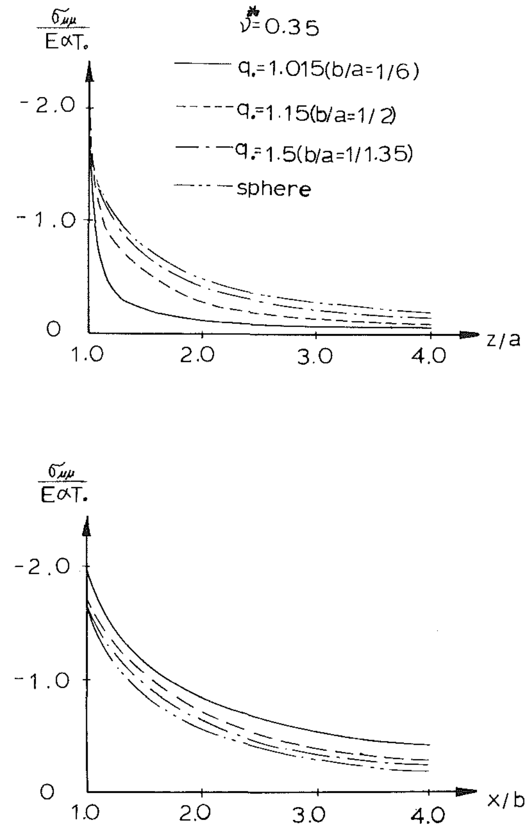

Fig. 6 Nondimensionalized stress $\sigma_{\mu\mu}/E\alpha T_o$ along the z and x axes of the prolate spheroidal cavity

$$\bar{R}_2(q)=\frac{1}{21}\left[Q_o'(q)\,(3-21q^2)-14\right]$$

$$\bar{R}_4(q)=\frac{2}{35}\,Q_o'(q)$$

where $\beta=\dfrac{1}{6}\,\dfrac{(1+\nu^*)}{(1-\nu^*)}\,\dfrac{\alpha T_o}{Q_o(q_1)}$, and $\dfrac{1}{h^2}=\delta^2(q^2-p^2)$

where A_n and B_n are constants determined from the traction-free cavity surface boundary conditions. The resulting stress fields generated by those functions have been detailed in reference [9] and are not repeated here. The requirement that the superposed solution for $\sigma_{\lambda\lambda}$ and $\sigma_{\lambda\nu}$ vanishes at $q=q_o$ yields $A_n=0$(n odd), $B_n=0$ (n even) and the following set of algebraic equations

$$\begin{array}{llll}
b_oA_o+a_2A_2 & +\beta_1B_1+\alpha_3B_3 & & =-\beta R_o\\
c_oA_o+b_2A_2+a_4A_4 & +\gamma_1B_1+\beta_3B_3 & +\alpha_5B_5 & =-\beta R_2\\
\bar{c}_oA_o+\bar{b}_2A_2+\bar{a}_4A_4 & +\gamma_1B_1+\bar{\beta}_3B_3 & +\bar{\alpha}_5B_5 & =-\beta\bar{R}_2\\
c_2A_2+b_4A_4+a_6A_6 & & +\delta_1B_1+\gamma_3B_3+\beta_5B_5+\alpha_7B_7 & =-\beta R_4\\
\bar{c}_2A_2+\bar{b}_4A_4+\bar{a}_6A_6 & & +\bar{\delta}_1B_1+\bar{\gamma}_3B_3+\bar{\beta}_5B_5+\bar{\alpha}_7B_7 & =-\beta\bar{R}_4
\end{array}$$

The stress components generated by χ_p vanish at infinity. However, the thermo-elastic stresses $\sigma_{\lambda\lambda}$ and $\sigma_{\lambda\nu}$ at the cavity surface $q=q_o$ have to be annulled by superposition with the corresponding homogeneous solution.

The homogeneous solution is sought from the Papkovitch-Neuber form for the axisymmetric, isothermal displacement field corresponding to the homogeneous field defined by

$$\mathbf{u}_H=\mathbf{u}_1+\mathbf{u}_2 \tag{19}$$

with

$$\mathbf{u}_1=\delta^2\,\nabla\,\phi,\ \mathbf{u}_2=\delta z\,\nabla\,\psi-\mathbf{k}(3-4\nu^*)\delta\psi$$

where $\nabla^2\phi=0$, $\nabla^2\psi=0$, and $\mathbf{k}$ is a unit vector along the z-axis of the spheroid.

The harmonic functions ϕ and ψ admit a Fourier-Legendre series representation in the form

$$\begin{aligned}\phi&=\delta^2\sum_{n=0}^{\infty}A_nQ_n(q)P_n(p)\\ \psi&=\delta\sum_{n=1}^{\infty}B_nQ_n(q)P_n(p)\end{aligned} \tag{20}$$

for $n\geq 6$, n even

$$\begin{aligned}&c_{n-2}A_{n-2}+b_nA_n+a_{n+2}A_{n+2}+\delta_{n-3}B_{n-3}+\gamma_{n-1}B_{n-1}\\ &\qquad+\beta_{n+1}B_{n+1}+\alpha_{n+3}B_{n+3}=0\\ &\bar{c}_{n-2}A_{n-2}+\bar{b}_nA_n+\bar{a}_{n+2}A_{n+2}+\bar{\delta}_{n-3}B_{n-3}+\bar{\gamma}_{n-1}B_{n-1}\\ &\qquad+\bar{\beta}_{n+1}B_{n+1}+\bar{\alpha}_{n+3}B_{n+3}=0\end{aligned} \tag{21}$$

The values of the coefficients a_n, b_n, c_n, α_n, β_n, γ_n, δ_n, $\bar{a}_n$, $\bar{b}_n$, $\bar{c}_n$, $\bar{\alpha}_n$, $\bar{\beta}_n$, $\bar{\gamma}_n$, $\bar{\delta}_n$, are identical to those in reference [9]. In contrast, it is noteworthy that $A_n=0$ (n even), $B_n=0$ (n odd) for the assumed boundary conditions in reference [9] with radically different thermal forcing terms.

The coefficients A_n and B_n are numerically calculated by using a preselected finite number of equations from the foregoing linearly independent system equations. The resultant stress solutions typically have the form

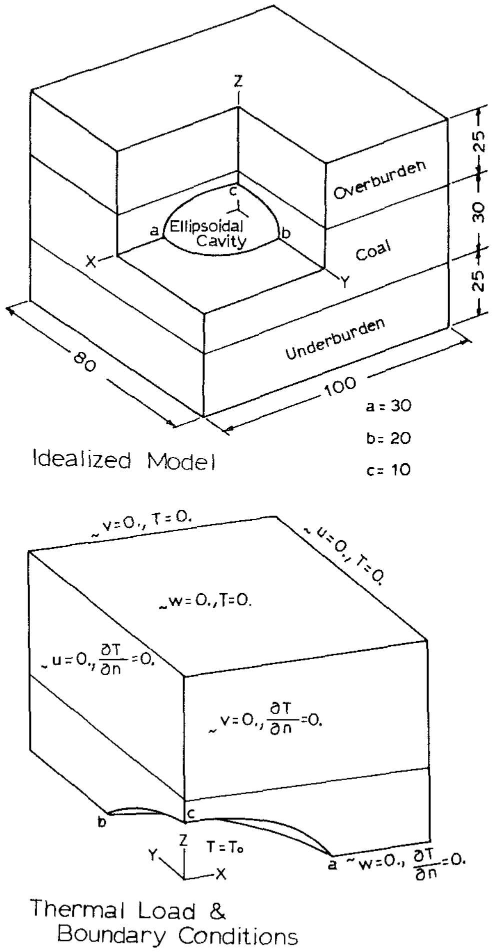

Material Properties				
	E GPa (kpsi)	ν	α μm/mC (10^6 ft/ft·F)	k mW/mC (10^5 Btu/F·ft·s)
Coal	1.282 (186.)	0.44	5.004 (2.780)	206.4 (3.348)
Rock	13.790 (2000.)	0.12	8.100 (4.500)	186.9 (3.000)

Fig. 7 Idealized ellipsoidal cavity layered model for finite element simulation

$$\frac{\sigma_{\lambda\lambda}}{2\mu^* \delta^4 h^4} = \beta[R_o(q)P_o(p) + R_2(q)P_2(p) + R_4(q)P_4(p)] + n^{\Sigma}\text{even}\, A_n[a_n(q)P_{n-2}(p) + b_n(q)P_n(p) + c_n(q)P_{n+2}(p)] + n^{\Sigma}\text{odd}\, B_n[\alpha_n(q)P_{n-3}(p) + \beta_n(q)P_{n-1}(p) + \gamma_n(q)P_{n+1}(p) + \delta_n(q)P_{n+3}(p)]$$

The convergence characteristics of the normal stresses $\sigma_{\lambda\lambda}$, $\sigma_{\mu\mu}$, and $\sigma_{\nu\nu}$ along the principal axes of the prolate spheroid were numerically checked for a 10×10 and 16×16 matrix resulting from two different truncations of equations (18). The results for the stress components for these two truncations revealed less than a 1-percent difference for the selected prolate spheroid geometries. Numerical results illustrating the nondimensionalized stress profiles along the cartesian axes (x,z) for different prolate spheroid shape ratios and $\nu^* = 0.35$ are illustrated in Figs. 4, 5, and 6. All the curves correspond to the solution of a 10×10 matrix with the values of $A_o, A_2, A_4, A_6, A_8, B_1, B_3, B_5, B_7$, and B_9 solved for the truncated set of equations (18).

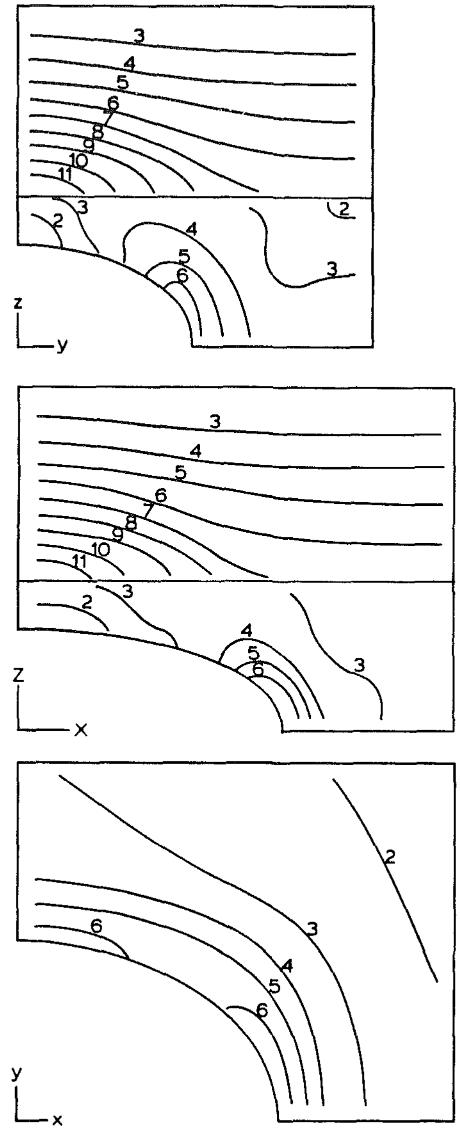

Fig. 8 Nondimensional maximum principal stress ($\sigma/E\alpha T$) contour plots for principal cartesian coordinate planes

Finite Element and Failure Criteria Simulation

The preceding results serve as benchmarks for subsequent sophisticated finite element modeling. Complicating effects such as multi-layering, temperature-dependent properties, and moving boundary conditions due to progressive combustion and/or failure zones can be incorporated in these simulations [23]. The thermo-elastic solution for the case of an ellipsoidal cavity in an elastic, isotropic infinite medium has been successfully calibrated against its finite element counterpart prior to finite element evaluations for the layered problem. As an example, Fig. 7 illustrates a confined ellipsoidal cavity model representing an intermediate stage during underground coal conversion. The assumed boundary conditions and material properties are also indicated. Figure 8 illustrates the normalized maximum principal stress ($\sigma/E\alpha T$) contour plots, using an in-house developed code, in the principal planes. The jump in the normal stress magnitudes at the coal-overburden interface is a result of the elastic modulus mismatch. These results when superposed with the gravitational loading effects provide basic information on stress mediated cavity growth. Additional illustrations revealing a comparison between the stress intensity factors governed by equations (10) and (11) and corresponding finite element formulations (Figs. 9(a,b)) have also been conducted.

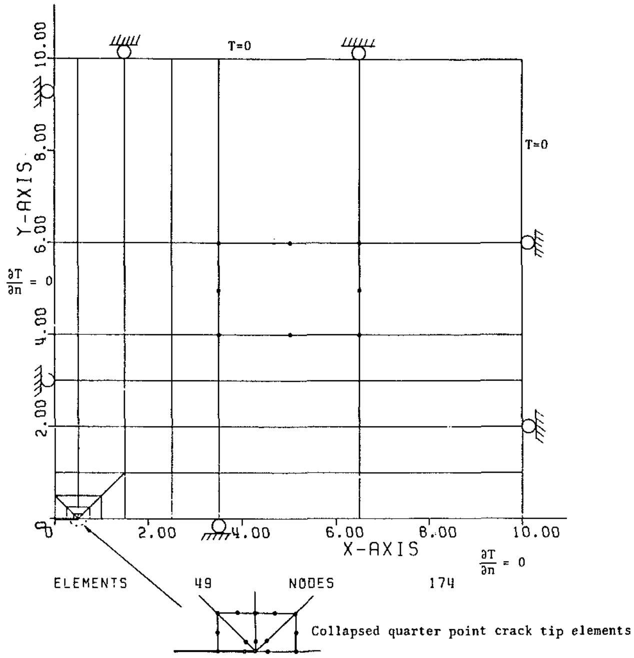

Fig. 9(*a*) Finite element mesh and boundary conditions for K_I problem

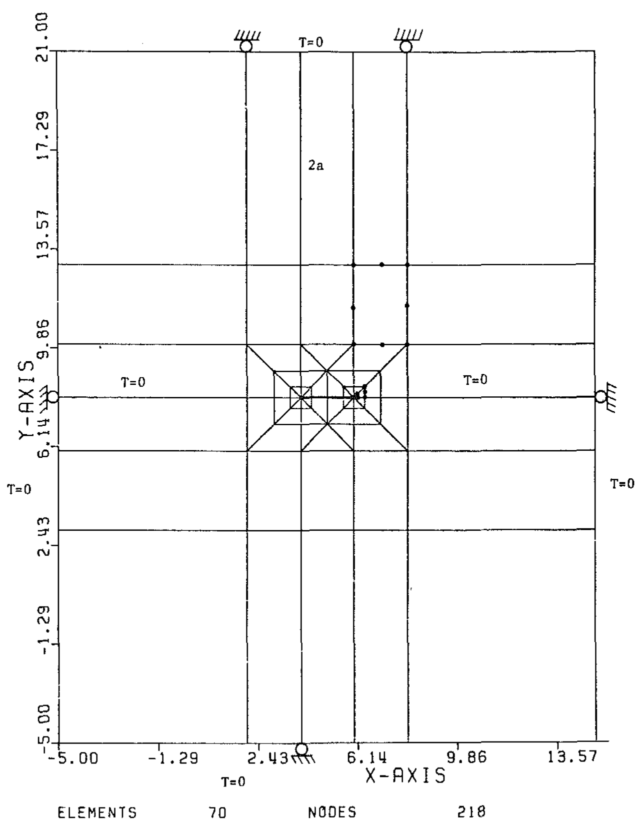

Fig. 9(*b*) Finite element mesh and boundary conditions for K_{II} problem

Eight node degenerate finite elements are utilized for these thermally loaded crack response computations with collapsed six-node triangular elements around the crack tip. The finite element results yield

$$K_I / \frac{(1+\nu^*)}{(1-\nu^*)} \alpha\mu^* T_o (\pi b)^{1/2} = 1.0204$$

and $K_{II} / \dfrac{(1+\nu^*)}{(1-\nu^*)} \alpha\mu^* (\nabla T) b^{3/2} = -1.0525.$

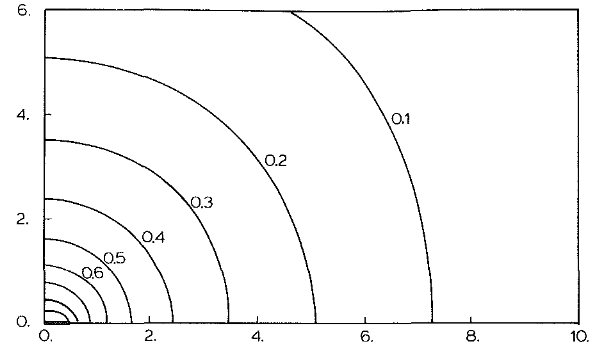

Fig. 10(*a*) Nondimensional temperature (T/T_o) contour plots for K_I problem

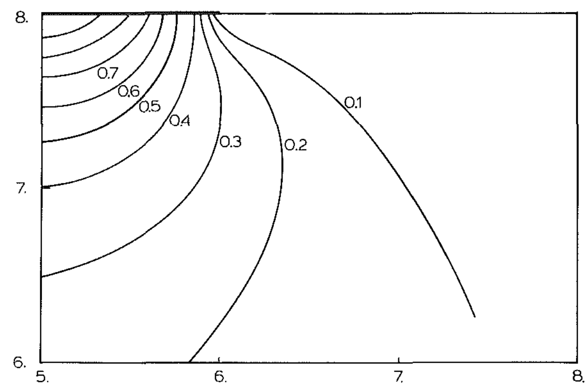

Fig. 10(*b*) Nondimensional temperature ($T/(\nabla T)b$) contour for K_{II} problem

Associated temperature and maximum principal stress plots are shown in Figs. 10 and 11.

Pertinent two and three-dimensional thermo-elastic failure criteria, incorporating the effects of crack/cavity closure, have been developed by Advani and Lee [24]. The two-dimensional thermo-mechanical failure condition in terms of the principal stresses σ_1, σ_3 can be expressed in the form [24]

$$\begin{aligned}(\sigma_1-\sigma_3)(1+\mu_f^2)^{1/2} - \frac{4A_I}{b} + \mu_f[\sigma_1+\sigma_3+2p_o \\ -2(3\alpha M T_o+\sigma_c)] \\ = 4S_t[1-\frac{(3\alpha M T_o+\sigma_c+p_o+2A_R/b)]^{1/2}}{S_t}\end{aligned} \tag{22}$$

where μ_f is the internal coefficient of friction, p_o is the crack pressure, M is the bulk modulus, σ_c is the critical stress for crack closure, S_t is the tensile strength, and the constants A_R and A_I are defined in terms of the thermally induced stress intensity factors by the relations $K_I = 2A_R\pi^{1/2}/b^{1/2}$ and $K_{II} = -2A_I(\pi)^{1/2}/b^{1/2}$. The results of McClintock and Walsh [25] can be deduced from equation (22) by ignoring thermal and crack pressure effects ($A_R = A_I = 0$, $p_o = 0$). Alternatively, a thermo-mechanical criterion, with crack closure and frictional effects, in terms of the Modes I and II stress intensity factors has been developed [24]. The fracture envelop is governed by

$$\frac{K_I}{K_{Ic}} + \left(\frac{K_{II}}{2K_{Ic}}\right)^2 = 1 \tag{23}$$

Good agreement between the experimentally determined values and theoretical predictions have been obtained.

Conclusions and Recommendations

The techniques and results presented here provide the rock mechanics researcher sophisticated tools for (*i*) thermo-

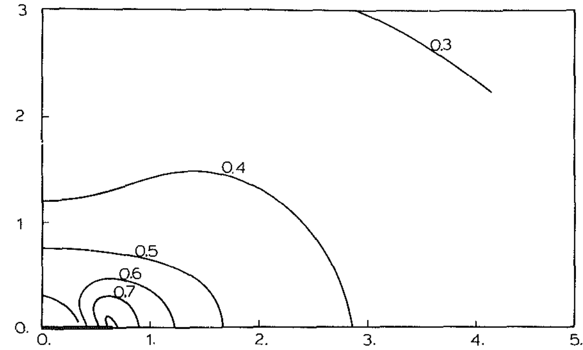

Fig. 11(*a*) Nondimensional maximum principal stress plots ($\sigma_{max}/E\alpha T$) for K_I problem

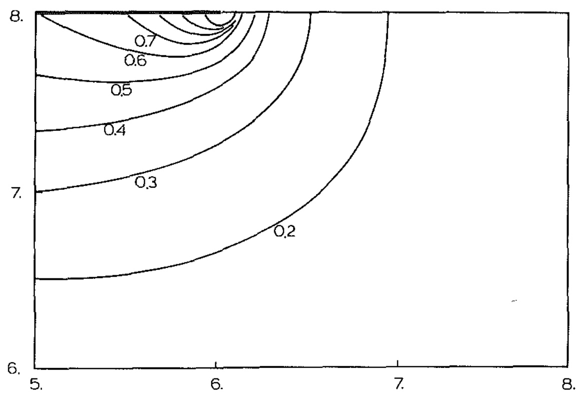

Fig. 11(*b*) Nondimensional maximum principal stress plots ($\sigma_{max}/E\alpha(\nabla T)b$) for K_{II} problem

elastic response prediction, (*ii*) comparison of results with special cases, and (*iii*) assignment of appropriate failure criteria for evaluation critical zones. Current areas of application include energy recovery from underground coal gasification, oil shale retortion, tar sands, geothermal reservoirs and subsidiary areas related to nuclear waste disposal and permafrost.

Extension of the numerical models to investigate thermo-poro-elastic effects [26] and associated nonisothermal consolidation is still in infancy. The development of comprehensive finite element codes introducing coupled phenomena along with suitable constitutive properties, transient behavior, thermo-visco-plastic creep, joint fracture systems including bi-material interfaces, and ablating boundary conditions should be systematically incorporated in various subroutines.

Acknowledgments

The financial support of the Laramie Energy Technology Center, U.S. Department of Energy through Contract No. DE-AC-20-80LC10335 is gratefully acknowledged. Computational assistance was provided by Mr. S. Lee and Mr. O. K. Min.

References

1 U.S. Department of Energy, "Underground Coal Conversion—Program Description," DOE/ET-0100, June 1979.

2 Tyner, C. E., and Hommert, P. J., "Numerical Modeling of a True In-Situ Oil Shale Retort," Sandia National Laboratories Report, SAND 78-1307, Jan. 1979.

3 Closmann, P. J., and Phocas, D. M., "Thermal Stresses Near a Heated Fracture in a Transversely Isotropic Medium," Society of Petroleum Engineers of AIME, Paper No. SPE 6183, 1976.

4 Smith, M. C., Potter, R., Brown, D., and Aamodt, R. L., "Induction and Growth of Fractures in Hot Rock," *Geothermal Energy*, eds., P. Kruger and C. Otts, Stanford University Press, 1973.

5 Tsang, C. F., and Wang, J. S. F., "State-of-the-Art of Models for Geothermal Processes," ASME Journal of Energy Resources Technology, Vol. 103, 1981, pp. 291–295.

6 U.S. National Committee for Rock Mechanics," Rock-Mechanics Research Requirements for Resource Recovery, Construction and Earthquake-Hazard Reduction," National Academy Press, Washington, D.C., 1981.

7 Myklestad, N. O., "Two Problems of Thermal Stresses in the Infinite Solid," ASME *Journal of Applied Mechanics*, Vol. 64, 1942, pp. A136–A143.

8 Edwards, R. H., "Stress Concentrations Around Spheroidal Inclusions and Cavities," ASME *Journal of Applied Mechanics*, Vol. 18, 1951, pp. 19–30.

9 Florence, A. L., and Goodier, J. N., "Thermal Stresses Due to Disturbance of Uniform Heat Flow by an Insulated Ovaloid Hole," ASME *Journal of Applied Mechanics*, Vol. 27, 1960, pp. 635–639.

10 Florence, A. L., and Goodier, J. N., "Thermal Stress Due to Disturbance of Uniform Heat Flow by an Insulated Spheroidal Cavity," *Proceedings of the 4th U.S. National Congress on Applied Mechanics*, Vol. I, Berkeley, 1962, pp. 595–602.

11 Sih, G. C., "On the Singular Character of Thermal Stresses Near a Crack Tip," ASME *Journal of Applied Mechanics*, Vol. 29, 1962, pp. 587–589.

12 Sekine, H., "Thermal Stress Problems for a Ribbon-Like Inclusion," *Letters in Applied and Engineering Sciences*, Vol. 5, 1977, pp. 51–61.

13 Sekine, H., "Thermal Stress Singularities at Tips of a Crack in Semi-Infinite Medium Under Uniform Heat Flow," *Engineering Fracture Mechanics*, Vol. 7, 1975, pp. 713–729.

14 Shindo, Y., and Atsumi, A., "Thermal Stresses in a Laminate Composite with Infinite Row of Parallel Cracks Normal to the Interfaces," *International Journal of Engineering Science*, Vol. 13, 1975, pp. 25–42.

15 Olesiak, Z., and Sneddon, I. N., "The Distribution of Thermal Stress in an Infinite Elastic Solid Containing a Penny-Shaped Crack," *Archives of Rational Mechanical Analysis*, Vol. 4, 1959, pp. 238–254.

16 Kassir, M. K., and Sih, G. C., "Three-Dimensional Thermo-Elastic Problems of Planes of Discontinuities on Cracks in Solids," *Developments in Theoretical and Applied Mechanics*, Vol. 3, 1967, pp. 117–146.

17 Kassir, M. K., "Thermal Stresses in an Elastic Solid Containing a Plane Crack," *International Journal of Engineering Science*, Vol. 13, 1975, pp. 703–711.

18 Kassir, M. K., "Thermal Crack Propagation," *Journal of Basic Engineering*, Vol. 93, 1975, pp. 643–648.

19 Advani, S. H., and Wang, H. F., "Thermoelastic Stresses Associated with a Triaxial Ellipsoidal Cavity," *Journal of Thermal Stresses*, Vol. 3, 1980, pp. 295–314.

20 Kassir, M. K., "The Distribution of Stress Around a Flat Parabolic Crack in an Elastic Solid," *Engineering Fracture Mechanics*, Vol. 2, 1971, pp. 373–385.

21 Wang, H. F., "Thermoelastic Solutions for In-Situ Gasification of Coal," Ph.D. dissertation, Department of Mechanical Engineering and Mechanics, West Virginia University, Morgantown, W.Va., 1978.

22 Muskhelishvili, N. I., "Some Basic Problems of Mathematical Theory of Elasticity," English translation, P. Noordhoff and Co., New York, 1953.

23 Advani, S. H., and Lee, J. K., "Structural and Fracture Mechanics Modeling Associated with Underground Coal Conversion," Final Report, Contract No. DE-AS20-80LC10335, The Ohio State University, Apr. 1981.

24 Advani, S. H., and Lee, K. Y., "Thermo-mechanical Failure Criteria for Rock Media," *Proceedings 20th U.S. Symposium on Rock Mechanics*, 1979, pp. 19–25.

25 McClintock, F. A., and Walsh, J. B., "Friction on Griffith Cracks in Rocks under Pressure," *Proceedings of the 4th U.S. National Congress on Applied Mechanics*, Vol. I, Berkeley, 1962, pp. 1015–1021.

26 Witherspoon, P. A., Tsang, Y. W., Long, J. C. S., and Noorishad, J., "New Approaches to Problems of Fluid Flow in Fractured Rock Masses," *Proceedings 22nd U.S. Symposium on Rock Mechanics*, 1981, pp. 1–20.